JOURNAL OF OPTOELECTRONICS AND ADVANCED MATERIALS Vol. 21, No. 1-2, January – February 2019, p. 74-92

Cracks in silicon photovoltaic modules: a review

A. ENNEMRI[a,b,*], P. O. LOGERAIS[b*], M. BALISTROU[a], J. F. DURASTANTI[b], I. BELAIDI[a]

[a]*Laboratory of Energy, Mechanical and Engineering, Faculty of Engineering Sciences, University of M'hamed Bougara (UMBB), Independance Avenue, 35000 Boumerdes, Algeria*

[b]*Université Paris-Est, CERTES, IUT de Sénart-Fontainebleau, 36 rue Georges Charpak, 77567 Lieusaint, France*

Photovoltaic cells are considered as one of the most critical components in photovoltaic systems for they convert the sunlight photons into electricity. However defects on the surface of the photovoltaic cells have a detrimental effect on them. Thus, research focuses on one hand on the degradation caused by the cracks namely on their impacts on the efficiency of photovoltaic modules and on the other hand on the techniques which are used to spot them. The main objective of this review is to inquire on the impact of the microcracks on the electrical performance of silicon solar cells and to list the most used detection techniques of cracks.

(Received July 9, 2018; accepted February 12, 2019)

Keywords: Photovoltaic module, Crystalline silicon cell, Cracks, Degradation, Crack detection

1. Introduction

Renewable energy sources are a viable alternative for clean energy production. Among these sources, solar photovoltaic energy has been the most vastly used and the most developed one for the last decade. According to the International Renewable Energy Agency (IRENA), 94 GW of photovoltaic capacity was installed in 2017 [1].

Under this leap of production, a large number of photovoltaic technologies are commercialized such as crystalline silicon, amorphous silicon and other thin film technologies like cadmium telluride (CdTe), copper-indium-selenide (CIS) and copper-indium-gallium diselenide (CIGS) cells. Crystalline silicon solar cell technology is at present broadly utilized in photovoltaic installations given that single crystalline silicon solar cells have a high conversion efficiency. The latter was measured at 25% under 1 kW/m^2 irradiance with AM1.5 spectrum at 25°C [2]. This technology is followed by polycrystalline cells which are simple to manufacture and less expensive but with lower efficiencies in the magnitude of 20% [3]. For the thin film technology, the most popular cells are the amorphous silicon (a-Si) solar cells with a conversion efficiency of around 12% in laboratory [2] and 5-7% under outdoor conditions [4]. It should be noted that the conversion efficiency for the CdTe technology is beyond 20% [2,5] and has lately been reported at 22% [6].

Each of these technologies suffers from performance degradation caused by the aging and the deterioration of the constitutive materials under operating conditions. The degradation of the photovoltaic modules and their reliability in field conditions have been a major research topic since the 1970s and had first been handled in the framework of the Flat Plate Solar Array project sponsored by the American energy department [6,7].

The degradation is defined as a gradual deterioration of the characteristics of a component or of a system which may affect its ability to operate within the limits of an acceptability criteria and which is aroused by the operating conditions [8]. The most frequent photovoltaic module degradation modes are:

–Yellowing;
– Delamination;
– Bubbles;
– Cracks in the cell;
– Defects in the anti-reflective coating;
– Burnt cells.

Scientific research has been focusing over the last decades on cracking in silicon solar cells and wafers, one of the predominant identified degradations of the crystalline silicon modules according to the NREL [8,9]. Cracks may develop at different stages of the lifetime of the module especially during manufacturing as the soldering induces high stresses into the solar cells [10–12]. Vibrations during transport while handling can lead to cracks or equally to expanding them [13,14].

There are three distinct sources of cracks during manufacturing. The most common one is when the residual stress pulled in by the soldering process induces cracks starting from the cell interconnect ribbon [15]. Cracks are indeed frequently located at the end or at the starting point of the connectors where the residual stress is the highest. Secondly, the cracks may be initiated by the needles which press on the wafers when in production. Finally, the bouncing of photovoltaic cells against a hard object while in the manufacturing process frequently engenders cracks commencing at the edge of the cell.

Owing to the remarkable technological progress at the material level, the photovoltaic industry has been experiencing a very rapid development. The size of the solar cells has been reduced for the last 15 years to lower their costs [16]. The thickness of the solar cells has been decreased from 300 μm to less than 150 μm or even to under 100 μm on production lines and at the same time

their surface has been raised to 210 mm × 210 mm. These changes have rendered the cells more brittle and susceptible to fracture while handling, storage and lamination of the module [15–17]. In parallel to this development, effective means to detect faults would be worth elaborating to carry out reliable and cost-effective inspections to avoid cellular defects.

The cracking problem has now become crucial as before the years 2000, it was not considered as a quantitative indicator for evaluating the quality of photovoltaic modules. To ensure the reliability of the manufactured cells, laboratory tests with guidance from field experience are performed such as [19]:

- Extending the time or cycles of the same tests used in the qualification test sequence;
- Increasing/decreasing the acceleration factors in the same tests used in the qualification test sequence;
- Combining stresses during testing;
- Using different accelerated stresses that are not included in the qualification tests which may be indicated from field results.
- Using accelerated stress tests to precondition modules for outdoor exposure.

Complementary tests like snow tests and artificial aging in laboratory using the electroluminescence technique for characterization revealed that microcracking of solar cells can lead to large electrically disconnected cell areas [20], with up to 16% of power loss [21]. In addition to laboratory tests on single panels, published field data disclosed that microcracked cells have non-constant current-voltage characteristics in time and an undesirable increase of the operating temperature [22].

The present article is a literature review on the origins and the characteristics of cracks in photovoltaic modules and wafers. It also provides an indepth note on the commonly used detection techniques for silicon solar cells. The impact of the cracks on the performance of a photovoltaic array and the different approaches to detect their presence are described. Thereafter, the outcomes of the studies and the various detection techniques are discussed with some solutions.

The article is organized as follows. First, a description of a classical silicon photovoltaic cell is done. Then, the origins, the causes of appearance and the classification of cracks within a silicon photovoltaic cell are explained. Next, the methods used by researchers to reproduce cracks and study their behaviours under different tests are given. The consequences on the electrical characteristics of a photovoltaic module are shown. Finally, before summing up the work, the main techniques employed to detect the microcracks are depicted with a comparison.

2. Description of a silicon photovoltaic module

Photovoltaic modules are multilayer systems as depicted in Fig. 1. The first layer L1 is the back contact in other words the backsheet, which includes a metal material, generally a tedlar/aluminium/tedlar stack acting as a conductor. The two following layers are the doped semiconductor materials. For a silicon cell doped with bore and phosphorus, the L2 layer p-type doped has a deficit of electrons, while the L3 one n-type doped has an excess of electrons. An electrical field and a difference of potential are induced in the contact zone of both these layers. The exposure of the semiconductor junction to solar radiations creates an excess of electrical charges for both the layers enabling to separate the positive charges from the negative ones. The grid L4b is placed in contact with the semiconductor surface. The grid is made of metal and functions as an electron collector and conductor. The anti-reflective layer L4a aims at maximizing the light that reaches the active region of the cell. The materials used are silicon dioxide and silicon nitride with cone or pyramid texture. The last layer L5 protects the cell with an encapsulation made either with glass or a polymer or both.

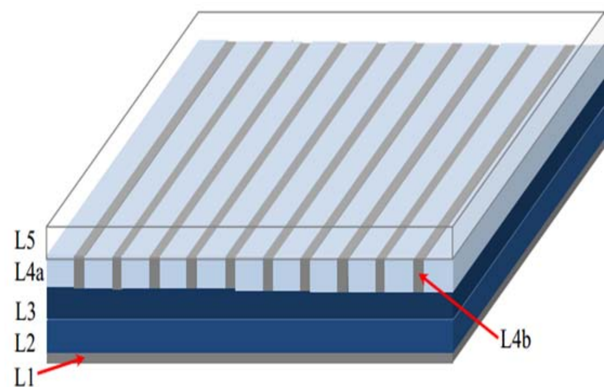

Fig. 1. Structure of a solar cell [23]

A solar cell is represented by an equivalent circuit composed of a current source (I_{ph}), a diode (D), a shunt/parallel resistance (R_{sh}) and a series resistance (R_s) as depicted in Fig. 2. The basic idea is to consider the photovoltaic effect as a source of a photogenerated current due to the movement of electrons and holes in the PN junction. The recombinations in the PN junction are modelled with one or two diodes [22].

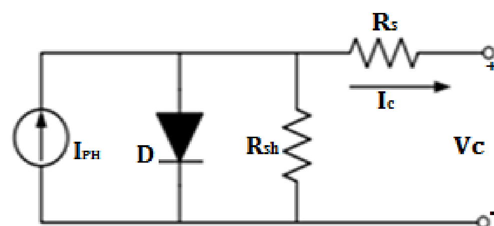

Fig. 2. Equivalent circuit for a solar cell [22]

Equation (1) gives the current-voltage response of a photovoltaic module with silicon cells connected in series [20–22]:

$$I = I_{ph} - I_s \left[\exp\left(\frac{V/n + R_s.I}{a.k.T} \right) - 1 \right] - \frac{V/n + R_s.I}{R_p} \quad (1)$$

where:

n is the number of cells,

I_{ph}, I_s and I are the photogenerated current, the saturation current and the module terminal current respectively (A),

V is the module terminal voltage (V),

R_s and R_p are the series resistance and the parallel resistance respectively (Ω)

a is the diode quality factor for polycrystalline silicon cells,

k is the Boltzmann's constant $\left(k = 1.3806503\times10^{-23}\ J/K\right)$,

T is the ambient temperature (K).

3. Cracking in photovoltaic modules

The cracks in the photovoltaic cells may emerge during the transportation or the installation of panels and also under particular operating conditions such as snow loads, strong winds and hailstorms [23–25].

Cracks can be observed at the start and at the end of the busbars, along them and on the surface of the cell [20,26]. They can have distinct sizes and orientations in a photovoltaic solar cell. They are categorized as microcracks when the size is inferior to 30 µm in width and as macrocracks when the critical length of 1 cm is reached [27]. They can also be classified according to their relative orientations regarding the busbar: parallel, perpendicular, dendritic or with several directions. The cracks open at the surface of a silicon wafer are reported as facial cracks, whereas when they extend or spread down towards the deepness of a wafer, they are called sub-facial cracks.

In field applications or during transportation, photovoltaic modules can be submitted to high temperatures, mechanical loads or other constraints, all of which prompt the appearance of cracks [28]. In the framework of laboratory tests, the cracks are introduced by diverse methods. The most prevalent means to reproduce cracks is the mechanical load test described in the IEC 61215 10.16 standards [29] which is useful to determine the ability of a unit to withstand stresses due to wind or static loads of snow or ice. A load corresponding to 2400 Pa is gradually applied to the front of the module to simulate a wind pressure of 130 km/h (approximately ± 800 Pa) with a safety factor of 3 for evenly distributed gusty winds. The load can be obtained pneumatically or by means of a weight covering the entire surface. In the latter case, the module must be mounted horizontally. If the module has to be qualified to withstand heavy accumulations of snow and ice, the load applied to the front of the module during the last cycle of this test is elevated, from 2400 Pa to 5400 Pa.

There exists as well the hail test to give an indication of the state of the photovoltaic modules when subjected to the impact of hailstones. This test is carried out by using suitable moulds for the casting of spherical ice balls of the required diameter for the projection with a determined test speed. A launcher capable of propelling an ice ball at the precise velocity is employed so as to hit the module within the designed impact location. The path of the ice ball from the launcher to the module may be horizontal, vertical or at any intermediate angle. The standard diameter used is of 25 mm with a test speed of 23 $m.s^{-1}$ but other diameters can be specified for special environments [29].

Moreover, there are tests where the load is applied per specimen called strength testing or four point bending. For the latter case, four point flexure devices are put to use to check out the wafer and the cell. They contain two bandings beam / rolls with two adjustable compression dies which can be used with a load. The test specimens are supported by two rolls at their bottom side and are loaded by two rolls on their top side [26,30].

Lastly, to create pre-existing cracks and study their evolution depending on the imposed flexure, moderate impacts were made with Poly Methyl Methacrylate (PMMA) balls of 4 cm diameter at a velocity of 6 m/s [31]. This way, cracks are introduced by an indentation effect.

4. Behaviour of cells and cracks under different tests

The cell cracks present in a photovoltaic module may spread in width and in length in the course of a functioning owing to mechanical and thermal stress. The consequences of applying tests reproducing the apparition and the development of cracks are analyzed here.

4.1. Mechanical load test

In the study of Kajari-Schröder et al., the standard IEC 61215 10.16 test was applied to 27 photovoltaic modules, the highest load being a 5400 Pa pressure [20]. The setup uses 5×3 suction cups uniformly distributed over the photovoltaic module to apply the push and the pull load. EL images were taken before and after the mechanical load test. The comparison of the two images highlights that 41% of the cells are cracked after the mechanical load test and that the distribution is as follows:

- 1% of the cracked cells broke perpendicular to the busbars which is the orientation giving the nominal risk of electrically separated cell area,
- 14% have dendritic cracks,
- 15% show several cracking directions,
- 20% have cracks with diagonal directions,
- 50% of the cracked cells have an orientation parallel to the busbars, which is the orientation of the greatest electrically separated cell area.

Another analysis of the criticality of the cracks formed during a uniform load test for determining the potentially separated cell area of these cracks revealed that cracks

parallel to the busbars frequently have a risk of separating cell areas within 16 to 25% [32].

Two distinct types of dark areas appeared in the electroluminescence (EL) images of silicon based solar cells after these tests: the irregular shaped areas represent cracks on silicon wafers and regular rectangular shaped areas stand for cracked or broken fingers on the front grid [33].

4.2. Strength testing

This method is used for examining both the strength of silicon wafers and silicon solar cells. The four point bending setup is most commonly employed for testing wafer strength. It loads homogeneously a large area by uniaxial bending moments including the surface and the edges of the sample. The results display that the layered structure can be considered having only a minor influence on the stiffness and on the stress distribution of the solar cells compared to a pure silicon wafer [34]. The strength of solar cells strongly relies on the loading direction caused by the metallization structure. For current standard solar cells, the sunny side evinces no influence on the loading direction. Otherwise, the backside exhibits different strengths depending on the loading direction. Concerning the crack development within the solar cell layers, the sunny side in tensile stress shows many more cracks compared to the backside in tensile stress. Nevertheless, the entire cell is not separated on all its thickness including the metallization. On the backside, higher fracture stresses occasioned the appearance of cracks related to the loading direction.

4.3. Humidity-freeze test

Photovoltaic modules are subjected to temperature cycles between 85°C and -40°C with relative humidity of 85% (according to IEC 61215) for this test used to check the coating resistance regarding the formation of cracks or the delamination due to heat in combination with humidity. After 200 humidity-freeze cycles, 29% of the cracked cells are degraded and only 7% of them develop an electrically disconnected cell area [32]. This separated area is in most cases lower than the threshold to affect the power output of the photovoltaic module. The results of this study also proved that about 40% of the cells are degraded with multiple crack orientations and 33% with parallel directions. A criticality analysis of these cracks pointed out that the probability of a part being electrically separated or degraded after an accelerated aging test strongly depends on the orientation of the crack.

4.4. Thermal cycling test

The photovoltaic modules are subjected to cycles between temperatures ranging from -40°C to 85°C for 200 cycles, with a maximum ramp rate of 100°C/h to check their resistance against the formation of microcracks. Down through these thermal cycles, the difference in the thermal expansion between the metal ribbon and the silicon wafer caused the disconnection of some fingers in the soldered cell [35]. Silicon has approximately a six time lower coefficient of thermal expansion compared to copper. It is then contracted, and the tin which has wicked along the finger is pulled back and upwards towards the copper ribbon. These factors create a crack.

The scanning electron microscopy (SEM) of a poorly welded cell revealed that the solder melts the ribbon for a certain distance along the fingers during welding which is an indication of over-soldering. The microcrack that is formed in the solder disconnects entirely the finger of the bar. Such a crack is susceptible to get widened during thermal cycling to totally disconnecting the metal finger [33]. The thermal fatigue has an impact along the grain boundary of the welding on the interconnection between the soldering copper and the silver metallization [26].

Fig. 3 illustrates some cracks for samples subjected to various accelerated stresses.

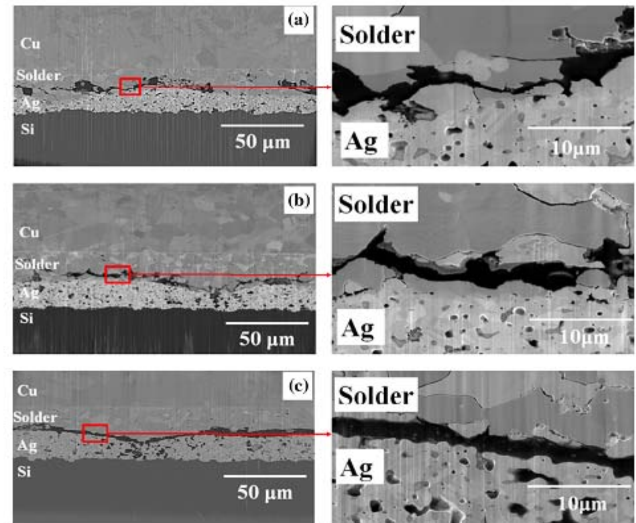

Fig. 3. SEM images illustrating the formation of cracks in the soldering interconnection: (a) -20 to 70°C; (b) -35 to 85°C; (c) -50 to 100°C [26]

The analogy between fracture mechanics and contact mechanics is elaborated because thermoelastic effects are quite complex. The difference in temperature between the damaged areas and the intact regions of a solar cell can lead to a considerable reduction of the crack opening. For small cracks, this could bring about the closure of the crack and a self-healing of the fissure with an increase in the thermal conductance [36]. The coupling between the elastic and the thermal field can be expressed by the equations of thermoelasticity, continuity and thermal conduction. Microcracks introduce additional thermal resistance. On one hand, the mechanical problem is described by:

$$\int_V \sigma^T(\nabla \delta u)\,dV = \int_V f^T(\delta u)dV + \int_V \bar{\sigma}^T(\delta u)\,dS + \int_S t^T(\delta g)\,dS \quad (2)$$

where:

σ is the stress vector,
u is the displacement vector,
f is the body force vector,
$\bar{\sigma}$ is the vector of prescribed tractions on the boundary,
$t = (\tau, \sigma)^T$ and $g = (gt, gn)^T$.

On the other hand, regarding the thermal problem, the equation can be written in transient regime in the absence of internal heat sources as below:

$$\int_V q^T (\nabla \delta T) dV = \int_V \rho_V C_V \dot{T} \delta T dV + \int_V \bar{q} \delta T dS + \int_S q \delta g_T dS \quad (3)$$

where:
ρ_V is the mass density $(kg.m^{-3})$,
C_V is the specific heat $(J.kg^{-1}.K^{-1})$,
$\bar{q}$ is the vector of prescribed normal heat fluxes.

Delamination of encapsulant materials in photovoltaic cells often emerges at regions of metallization. A recently developed metrology for measuring the adhesion energy of module interfaces was used to evaluate the adhesion of encapsulation of each material of the upper layers of a photovoltaic module [37]. It is grounded on fundamental concepts of fracture mechanics. The adhesion of ethylene vinyl acetate (EVA) encapsulant to screen-printed silver metallization was evaluated. The fracture energy of the EVA/silver interface (952 J/m^2) was ~70% lower than that of the EVA/antireflective (AR) coating (>2900 J/m^2) and ~60% lower than the one of the EVA to the surface of the cell (2265 J/m^2). After merely 300 hours of damp heat aging, the adhesion energy of the silver interface dropped to and plateaued at ~50–60 J/m^2 while that of the EVA/AR coating and EVA/cell remained mostly stationary. Elemental surface analysis highlighted that the EVA separates from the metallization in a purely adhesive manner, indicating that bonds at the interface were likely displaced in the presence of humidity and chemical products at elevated temperature, which in part accounts for the propensity of metalized surfaces to delaminate in the field.

5. Crack impact on the electrical characteristics of the solar cells

The fragility makes the solar cells prone to cracks under the diverse conditions engendering a decrease in the energy produced over the years [38] and also fast-forwarding degradations such as corrosion, delamination, hot spot and discoloration [39].

The power loss depends on the number of cracks and on their orientations, distributions and dimensions. The orientation, the distribution and the distinctive impacts of cracks on the output power of a photovoltaic module are depicted in Fig. 4.

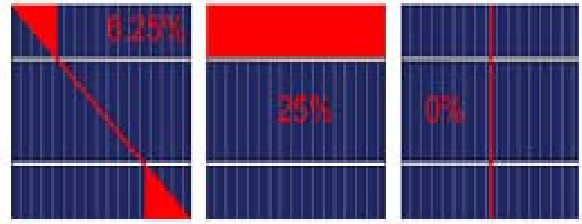

Fig. 4. Maximum power loss of a single crack for different orientations [20]

According to the study of Köntges et al., the risk of power loss of photovoltaic modules caused by microcracks after testing the mechanical load is less than 2.5% [40]. However, the cyclic thermal stress leads to fatigue cracks at the solder interconnection [41], which in turn increases the series resistance R_s of a photovoltaic module. The result of the augmentation of R_s is the lessening of the fill factor (FF). Consequently, the decrease of power generated by a solar cell can be attributed to the decrease of FF which is occasioned by the increase in R_s.

In addition to this power loss, all modules have high glass corrosion after a humidity freeze test [40]. Indeed, for all the cases of cell microcracks, a loss of cell surface greater than 8% leads to a substantial influence of this crack on the power output of the module.

To study the process of the expansion of microcracks in a crystalline solar cell under a thermal effect, the EL image can be used to determine the output characteristic as a function of the microcrack model. The I-V characteristics may be analyzed as a function of the crack growth model. Three distinct orientations for the cracks could be considered to obtain a mathematical modelling: perpendicular to busbar, parallel to busbar and diagonal to busbar [42]. The photocurrent may be written as a function of the current density J and of the total area A of the cell:

$$I_{ph} = J.A \quad (4)$$

So, the expression of the current output changes for each case depending on the defect region occasioned by cracking is:

$$I_{out} = J\left(A - A_{defect}\right) - I_0\left[\exp\left(\frac{q(V)}{nkT}\right) - 1\right] - \frac{V + IR_s}{R_{sh}} \quad (5)$$

where A_{defect} means a small region brought about by the crack.

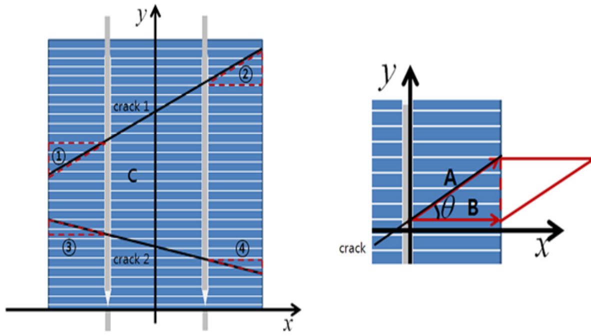

Fig. 5. Calculation of an inactive area using a cross product of vectors [42]

For the case of a microcrack diagonal to busbar, the inactive area is calculated using a cross product of vectors. As illustrated in Fig. 5, the vector product corresponds to the area of a parallelogram. Thus, the inactive region can be expressed as follows:

$$A = \frac{\|A\|\|B\||\sin\theta|}{2} \tag{6}$$

Song et al. developed an electric model to study the electrical characteristics of a photovoltaic module according to the cracked surface [42]. The error at the output between the measured values and the result of the model simulation was determined. Both the results were very close with a difference in the order of 3% as shown in Fig. 6.

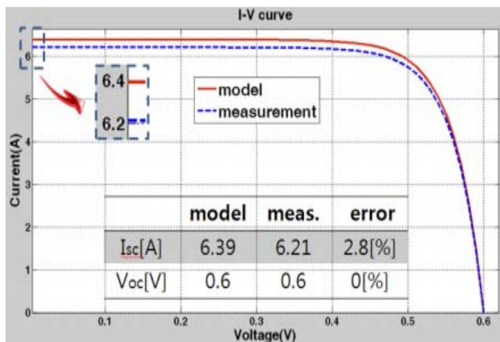

	model	meas.	error
Isc[A]	6.39	6.21	2.8[%]
Voc[V]	0.6	0.6	0[%]

Fig. 6. Comparison of I-V curve with theoretical prediction and experimental result [42]

A simulation study based on field data for the impact of cracks in multicrystalline silicon solar cells on photovoltaic module power estimated the power loss of the modules between 6 and 22% [43].

A multi-physics and multi-scale numerical approach permitted to study the evolution of microcracks in polycrystalline silicon solar cells composing photovoltaic modules and their effect on the electrical response [44]. This method took into account the microstructure of polycrystalline grains and the effect of grain boundaries which could be a source of microcracks. The intergranular cracks were simulated using a fracture mechanics model for the cohesive zone with the nonlinear finite element method.

To model the effect of cracking with regard to the electrical field, the saturation current (I_s) is considered linearly dependent on the electrically active cell area, as found in [44]:

$$D = \frac{A_{inactive}}{A_{Total}} \tag{7}$$

where:

$A_{inactive}$ is the inactive cell area (m^2),

A_{Total} is the total cell area (m^2).

The same definition applies to a photovoltaic module. The saturation current and the photocurrent become:

$$I_s = I_s^{D=0}(1-D) \tag{8a}$$

$$I_{ph} = I_{ph}^{D=0}(1-D) \tag{8b}$$

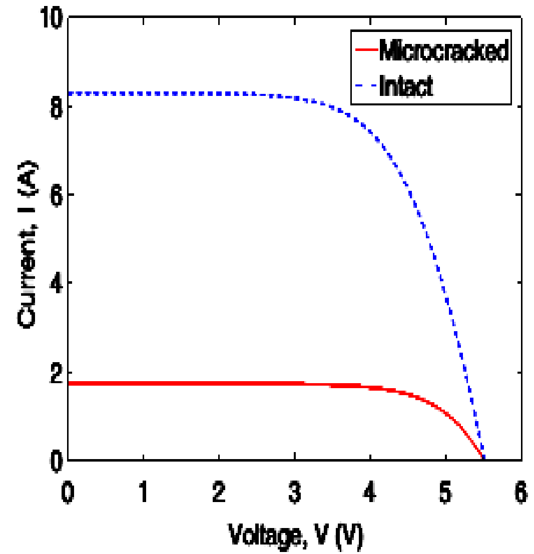

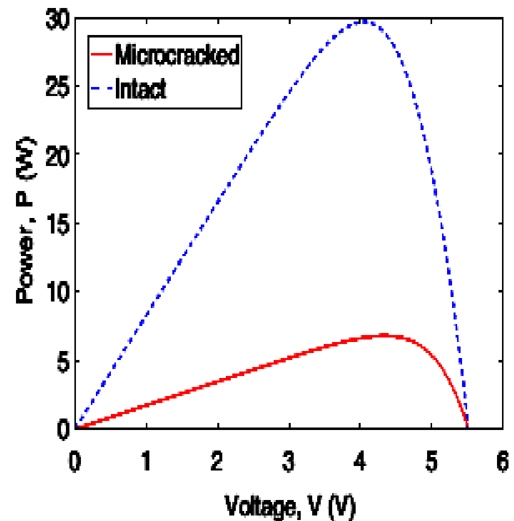

Fig. 7. Characteristic curves of intact and microcracked photovoltaic module [44]

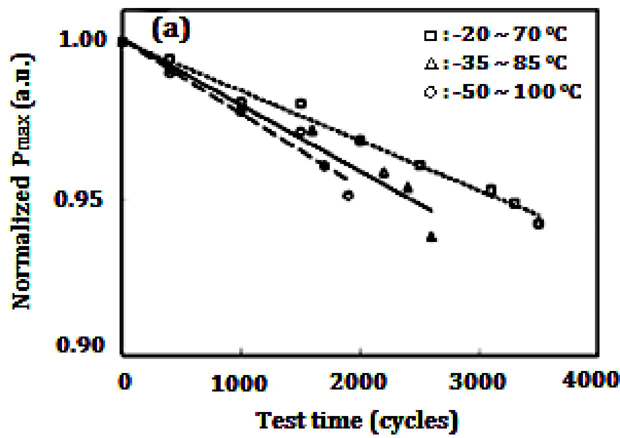

Fig. 8. Increase of the power loss according to the thermal cycles [26]

The numerical implementation revealed that the proposed approach can be applied in the real case [44]. The results for the electrical response of the intact and the cracked modules (D=79%) are displayed in Fig. 7.

The series resistance grows with each processing condition concerning a thermal cycle test [26]. The main impact of this raise is a diminution of the maximum power point P_{max} as given in Fig. 8.

Due to the encapsulation of silicon photovoltaic cells in a ductile polymer material, mechanical deformity influences the electrical field intensity as demonstrated by an experimental study based on the technique of electroluminescence [31].

Another experimental study revealed that only 60% of cracks had an important impact on the total amount of power generated by photovoltaic modules [45]. Only 15.6% of the overall photovoltaic modules examined had no cracks. The rest contained at least one type of crack: diagonal (26.7%), parallel to busbars (20%), perpendicular to busbars (8.9%) or cracks with multiple directions (28.9%). One should note that 60% of cracks have a substantial impact on the output power performance for all the screened photovoltaic modules. Fig. 9 shows that the significant cracks are present in 60% out of 84.4% of the cracked arrays.

An experiment to evaluate the impact of discoloured lines such as snail trails was carried out by Liu et al. [46]. The measured power reduction was greater than 5%. However, this research brings up that this loss is not related to the snail streaks but to the microcracks. A recent research mentioned that a photovoltaic cell with snail trails and another one with microcracks were closely related to each other [47]. It can be proven that the occurrence of snail trails indicates the presence of microcracks. The reduction in the maximum power point ranges from 10% to 30%.

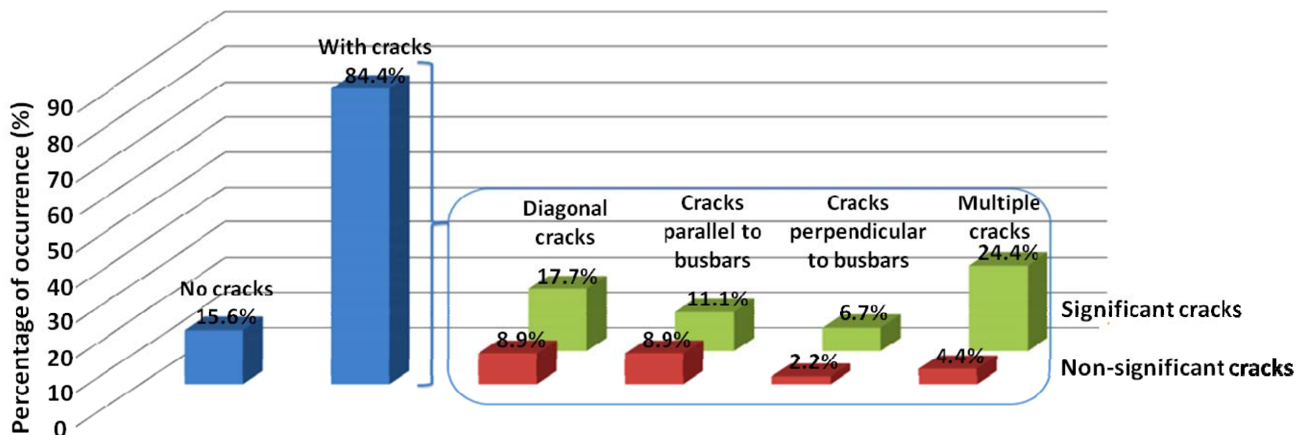

Fig. 9. Percentage of cracks in the examined photovoltaic modules [45]

6. Crack detection methods

The photovoltaic industry and research laboratories introduced tools for the characterization and the detection of defects under manufacturing processes and during operation. In this section, some Non-Destructive Techniques (NDT) and cross-sectioning techniques (Destructive Techniques, DT) are described.

The techniques reviewed hereafter are based on electrical, ultrasonic and sonic, optical and electromagnetic parameters plus thermography and infrared radiation.

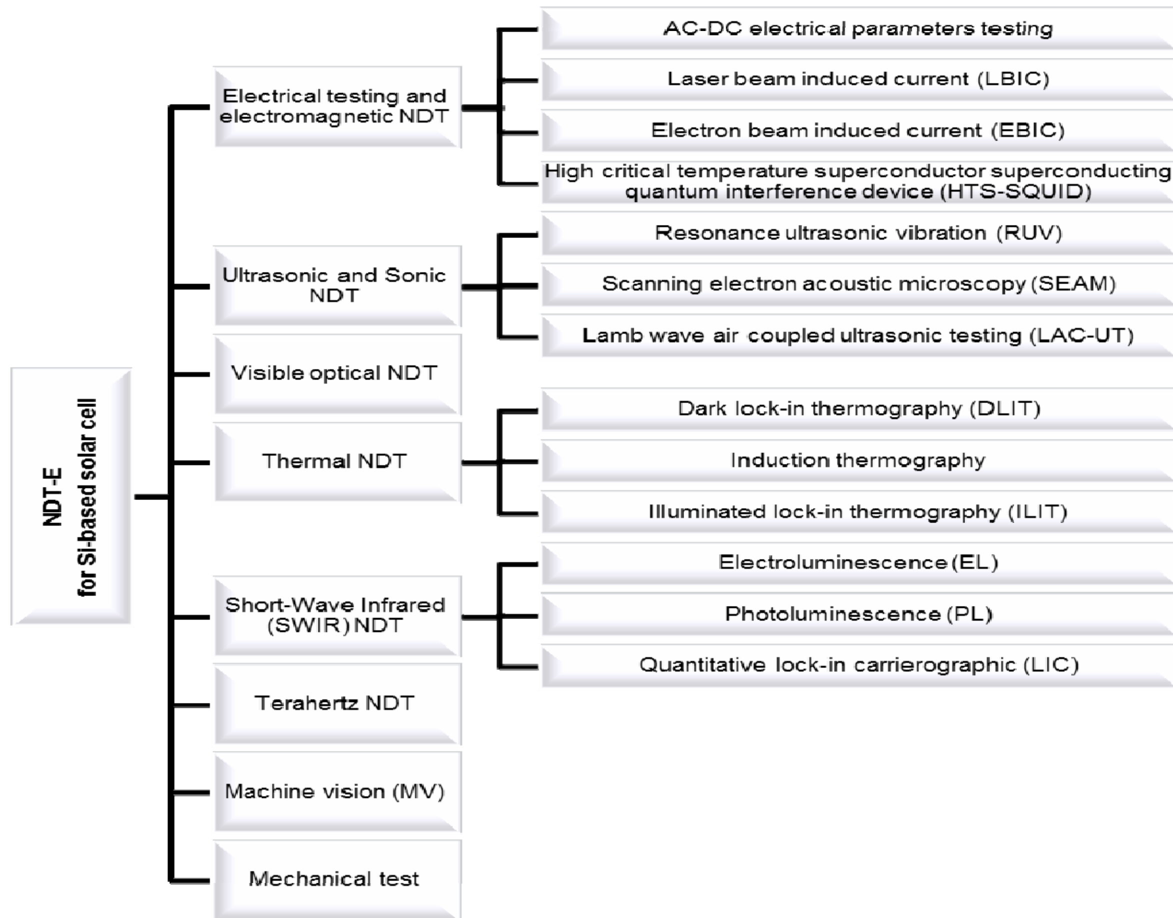

Fig. 10. NDT for silicon solar cell

6.1. Non-destructive technique

Non-destructive testing (NDT) is the process of inspecting, testing or evaluating materials, components or assemblies for discontinuities or differences in characteristics without destroying the serviceability of the cell or the system. The NDTs detailed below are classified in the chart of Fig. 10.

6.1.1. Electrical testing and electromagnetic NDT

Electromagnetic techniques are used to judge the internal damage and related properties of materials by the variation of electrical or magnetic properties.

6.1.1.1. Testing of DC-AC electrical parameters

The DC electrical parameters of solar cells play a major role not only in characterizing the solar cells or controlling their quality, but equally in the fabrication and in the evaluation of the power performance for reliable solar panels.

Nowadays, due to the development of new types of photovoltaic cells and of a large number of photovoltaic power plants, a growing number of published papers can be found on the methods to study the AC behaviour and to determine the AC parameters of solar cells and modules [40–46].

The equivalent circuit of a solar cell in the dynamic regime is obtained from the DC one diode equivalent circuit (Fig. 2) by replacing the diode with the diffusion capacitance C_d, the transition capacitance C_t and the dynamic resistance of diode R_d.

In addition, the dynamic equivalent circuit can be simplified using the parallel resistance combined with the parallel capacitance. The AC equivalent circuit and the simplified AC equivalent circuit for a solar cell are disclosed in Fig. 11.

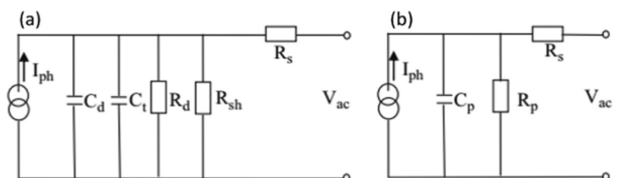

Fig. 11. The AC equivalent circuit (a) and the simplified AC equivalent circuit for a solar cell (b) [55]

The aging of a solar cell includes not only the electrical losses, but also the material deterioration influencing the rate of charge recombination and the bias in the PN junction. The same goes for cracking.

This method allows a thorough analysis of the behaviour and the dynamic performances of a photovoltaic system.

6.1.1.2. Laser beam induced current (LBIC)

LBIC technique is a notable method allowing the photocurrent response of a solar cell to be mapped [56]. It is employed under short-circuit current conditions and permits the calculation of the local diffusion length of the solar cell material from local photocurrent data.

A scheme of the LBIC apparatus is displayed in Fig. 12 [57]. It works with three excitation wavelengths supplied by a dual laser diode (639 nm and 830 nm laser lines) and a second laser diode (785 nm). The two laser beams are perpendicularly oriented.

A beam splitter directs the laser beams into a trinocular microscope, which is used to concentrate the excitation laser beam onto the sample surface. When a light beam is scanned over the surface of a photosensitive device, it creates electron-hole pairs in the semiconductor inducing a DC current which is in turn measured utilizing suitable devices [58]. Laser beam induced current methods have been investigated both for fast-line scan techniques and for detailed surface mapping [59]. The major drawback of the LBIC method is the necessity of electrical contacts making it nigh impossible to be applied to wafer inspections [60].

Furthermore, the scanning needs to be performed for the entire wafer area and this process is very time-consuming even though the accuracy of the LBIC is acceptable [61].

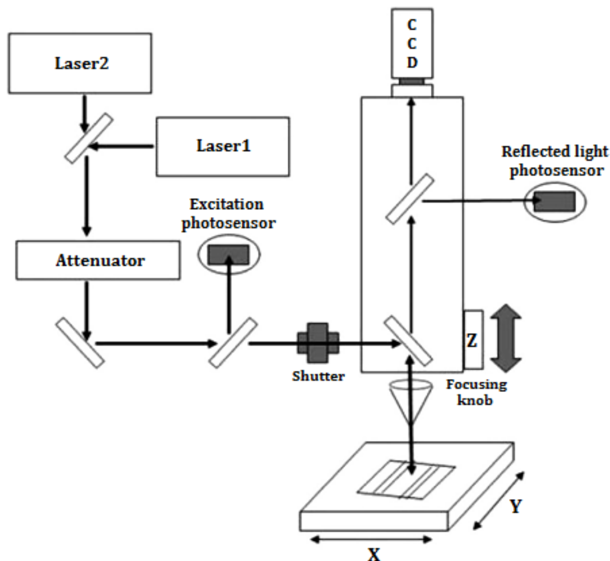

Fig. 12. System scheme LBIC [48]

6.1.1.3. Electron beam induced current (EBIC)

EBIC is an electrical defect characterization technique that detects recombination sites, doping level inhomogeneities and electrical irregularities in solar cells [62]. EBIC imaging is very sensitive to electron hole recombination [63] the reason for which the EBIC analysis is very useful in spotting defects that act as recombination centres in semiconductor materials. However, EBIC requires a PN junction and the detection range is limited to a few diffusion lengths from the junction.

EBIC currents are generally within the nanoampere to the microampere range while the primary beam current is in the picoampere magnitude. In regions around the PN junction where physical flaws exist, electron-hole recombination is enhanced, reducing then the collected current in such altered areas. Thereby, if the current through the junction is employed to produce the EBIC image, the areas with physical shortcomings will appear darker in the EBIC image than those without any.

EBIC imaging is thus a convenient tool for finding sub-surface and other difficult-to-see damage sites. The crack can be clearly seen in the image. Hence, this technique is useful to detect the presence or the absence of microcracks in solar cells or wafers.

6.1.1.4. High critical temperature superconductor superconducting quantum interference device (HTS-SQUID)

SQUID is an extremely sensitive instrument which can detect weak magnetic signals. It is used not only to measure changes in the magnetic flux, but also with other physical quantities such as voltage, current, resistance, inductance, magnetic induction, magnetic field gradient or magnetic susceptibility [64,65].

Thereupon, SQUID is a useful technique to evaluate the performance of solar cells, to measure the excitation current and to spot the presence of microcracks in solar cells [66].

6.1.2. Ultrasonic and Sonic NDTs

Ultrasonic and sonic NDTs are mostly employed in industries [67–69] and have a lot of members such as ultrasound-echo, phased/linear array ultrasonic, air coupled ultrasonic, laser ultrasonic and local resonance spectroscopy. Some of them have already been investigated for solar cell inspections by now [69].

Through the ultrasonic and solar cell interaction of reflection, transmission and scattering of the wave, the macro defect detection, geometry measurement, microstructure and the change in mechanical properties of solar cells can be detected and characterized and their performance can subsequently be evaluated [70].

6.1.2.1. Resonance ultrasonic vibration (RUV)

The technique was developed by A. Belyaev [71] and appears to be one of the most used methods in detecting cracks and microcracks.

It is grounded on the ultrasonic vibration analysis. This technique allows to detect the variations in the characteristic of the frequency response after an ultrasonic excitation of the wafer or of the silicon cell. The piezoelectric transducer emits ultrasonic vibrations

that produce sound waves vibrating the wafer or the cell. The limitation of this method is its sensitivity to the length and to the location of the crack as it permits to detect cracks up to the submillimeter lengths without knowing the exact place of the cracks. However, the method is widely used owing to the fact that it does not scratch the silicon surface and its speed of diagnosis is in the order of 2 seconds / cell or wafer. Nevertheless, this technique does not reveal the place of the crack [17,63]. The RUV relies on the deviation of the resonance frequency response curve measured on a wafer with peripheral or bulk millimetre-length crack from identical non-cracked wafers. Through a resonance frequency curve selected from a broad range (20–100 kHz), the RUV method enables crack detection with simple criteria for wafer or cell rejection.

Fig. 13 is a schematic diagram of an experimental RUV system.

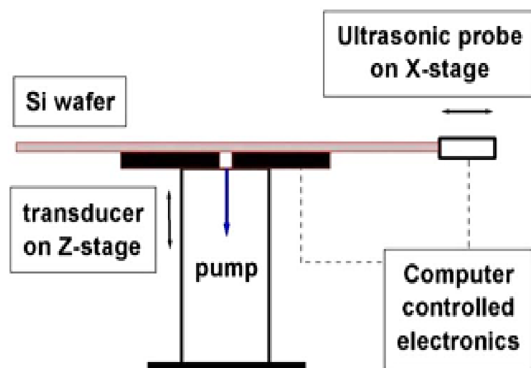

Fig. 13. A schematic of experimental RUV system [72]

6.1.2.2. Scanning electron acoustic microscopy (SEAM)

SEAM is a technique used for depth discrimination of multilevel integrated circuits and is applied for the characterization of morphological defects in solar cells [65–67].

It is based on the detection of electron acoustic signals that are generated within the multicrystalline (mc-Si) silicon wafer by a periodic intensity-modulated electron beam.

The principle is illustrated in Fig. 14. SEAM is utilized for the detection of facial microcracks where a focused high-frequency acoustic beam operating in a pulsed mode is scanned over the front surface of the wafer.

These pulses are transmitted through the silicon wafer at the velocity of the sound and are reflected at various interfaces, including the front and the back surfaces of the wafer.

The pulse echo technique operates at frequencies up to 250 MHz. The cracks are visualized through material discontinuities due to acoustic impedance mismatch caused by the microcracks. The duration needed to scan a 100 mm by 100 mm wafer is between 10 and 15 min making this method unsuitable for mass production. In addition, the wafer must be submerged in a water bath or covered with a water droplet because the high-frequency acoustic waves are attenuated quickly in air, requiring the placement of wafers in a coupling medium. This approach permits the detection of cracks as small as 5–10 µm.

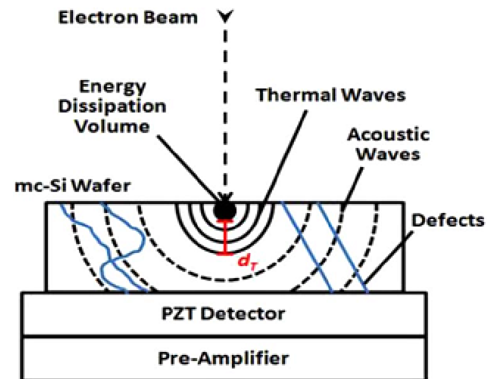

Fig. 14. SEAM signal detection from a mc-Si wafer [73]

6.1.2.3. Lamb wave air coupled ultrasonic testing (LAC-UT)

This technique can be used for crack detection in 200 µm thick silicon wafers at 200 kHz [74]. Mass production requirements of silicon wafer solar cells have raised significantly with a need to produce high quality flawless wafers in large volumes and at low costs [75]. There is a critical need for online inspection systems which can quickly catch weaknesses and are cost effective. Therewith, LAC-UT technique is greatly developed for detecting cracks in silicon wafers [76].

The ultrasonic energy travels through the thickness of the silicon wafer sample in the form of Lamb waves and is then converted back into electrical energy by the second air coupled transducer that acts as a receiver. The received signal from the air coupled transducer is amplified in series of stages by the inbuilt amplifier present in the receiver.

Monocrystalline and polycrystalline silicon wafers with defects of 20 µm size are uncovered by a LAC-UT system [74].

6.1.3. Visible optical NDT

Electronic speckle pattern interferometry (ESPI) technology is a non-contact real-time measurement technology in the audience because of its versatility, high accuracy, wide frequency range and simple measurement [77]. The ESPI non-destructive detection technology achieved rapid development and is able to pick the displacement, strain, surface defects and cracks [78]. It also enables to identify deformation on the specimen surface in accordance with its fringe pattern affected by the boundary conditions and by the original deformation of the specimen [79].

This method depends on the variation of the strain distribution due to the thermal deformation within the

solar cells brought on by discontinuities in the material properties or in the crystal lattice [80].

The ESPI image is taken from the back of the solar cells as ESPI is more suited for sensing rough surfaces instead of smooth ones. Furthermore, the charged couple device (CCD) camera signal is recorded by a personal computer. A temperature controllable planar heater is utilized to apply a heat flux to the object.

The edge-supported solar cell is heated to induce the bending deflection. Specklegram sensing is taken at constant temperature increments till speckle fringes near the crack become sufficient to determine the crack length.

6.1.4. Thermal NDT

Application of thermal imaging is very extensive: electricity, underground pipelines, fire, medical relief and industrial inspection have a huge market with the high technology development of social economy and the progress of science. The infrared thermal imaging is used in more fields as well [73,74,81].

The combination of a thermography system with noise reduction by a lock-in system has become an important tool in many areas of non-destructive testing of materials and devices [75,76]. There are two main types of lock-in thermography, namely, dark lock-in thermography (DLIT) and illuminated lock-in thermography (ILIT). The former is used by applying either a reverse bias to concentrate current in shunts or a forward bias to sense shunts. The latter uses light instead of voltage applied by contacts to drive currents through the shunts [82].

6.1.4.1. Lock-in thermography (DLIT/ILIT)

The principle of lock-in thermography is based on the application of a periodic or sinusoidal input energy wave (thermal emitter, ultrasound, microwave, eddy current, flash lamp) to the surface of the object being examined. The local temperatures on the surface of the object are analyzed.

Dark lock-in thermography (DLIT) technology refers to the solar cell with positive and negative bias (without external light irradiation) for which only the dark current flows in the solar cell [83]. DLIT was first proposed for solar cell inspection by Breitenstein et al. [84]. The latter also reported a quantitative study of the shunt resistance distribution on a solar cell using an infrared thermal camera [85]. Accordingly DLIT is extensively used for inspecting various types of solar cells.

ILIT is the first measurement technique that gives a quantitative and a spatially resolved measurement of the power losses in solar cells under operation conditions [86]. Originally, ILIT was mainly put to use under open-circuit condition (V_{oc}-ILIT) to investigate on the material quality and to carry out measurements on solar cells all along the cell manufacturing process [87]. Besides, it is operated at the maximum power point (MPP) to investigate the influence of distinctive deficiencies and cracks on the performance of solar cells.

Meanwhile distinguishable measurement modes, which were primarily tailored to the investigation of losses in series resistance on solar cells, evolved [88].

This technique has a high resolution but its limitation is its long acquisition time. Only cracks with triangular shape with large mouths at the surface and tiny tips are recognized. This method also suffers from thermal blurring.

6.1.4.2. Induction thermography

Induction thermography or eddy current pulsed thermography ECPT [82,83,89] uses electromagnetic pulses to excite eddy currents in electrically conductive materials. The eddy currents generate and release heat through resistive losses. The heat can be discerned on the surface by an infrared camera [90]. Surface cracks or hidden cracks neighbouring the surface brings up local moves of the electrical current densities becoming visible in the thermographic images [91]. The first applications of induction thermography or pulsed eddy current thermography were reported more than two decades ago in the steel industry [92].

6.1.5. Short-Wave Infrared (SWIR) NDT

6.1.5.1. Electroluminescence (EL)

The photographic surveying of electroluminescence (EL) under forward bias is proved to be a powerful diagnostic tool to inquire visually not merely on the material properties but also on the process induced deficiencies in silicon solar cells [93]. The EL image can distinctly highlight the barely visible faults as dark objects, showing at the same time random dark regions in the background, rendering automatic inspection with EL images very difficult [94].

The EL imaging system is a contact technique solely applicable for a finished solar cell [95]. The EL images are displayed as grayscale leading to difficulties in distinguishing the deficient areas. This fast and precise technique is superior to the conventional scanning method such as the LBIC one [93].

In this approach, solar cells are in the forward bias condition enabling them to emit infrared radiations. The luminescence ranges from 950 nm to 1250 nm with a peak occurring at approximately 1150 nm. Emission intensity is dependent on the density of flaws in the silicon, with fewer ones resulting in more emitted photons. The EL system should be placed in a dark room as the image of the cells has to be taken by the cooled charged couple device (CCD) camera.

Electroluminescence is classified as a contact technique. The imaging may be applied solely to the finished cell modules and solar panels. Another limitation is the interference with other deteriorations like scratches [96].

6.1.5.2. Photoluminescence (PL)

The image acquired by the photoluminescence technique is equally an infrared image as in the case of electroluminescence and thermography. Photoluminescence (PL) imaging was introduced by T. Trupke et al. [97]. The principle is to excite the electrons of the valence band with a higher energy photon to pass to the conduction band. The excitation thereupon sends the electrons to a more elevated state of energy before returning to a lower energy level with the emission of a photon.

The imaging setup is very similar to the EL one. The only discrepancy is that the electrons are excited by means of a laser source [98]. The system of detection based on the imaging photoluminescence is better than all the other systems and is ideally suited for automated production lines [99]. Fig. 15 shows the principle of this technique.

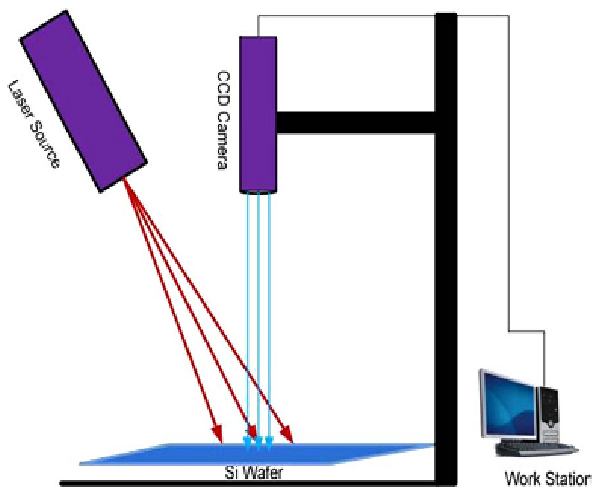

Fig. 15. PL measurement setup [99]

6.1.5.3. Quantitative lock-in carrierography (LIC)

Lock-in thermography (LIT) is available for the detection of shunts, series resistances and grain boundaries, and can be used to ascertain the power loss based on appropriate calibration [85].

Lock-in carrierography (LIC) is a non-contacting optoelectronic frequency-domain PL imaging method applied to quantify the solar conversion efficiency and the photoelectric voltage of industrial silicon solar cells [100].

6.1.6. Terahertz NDT

Terahertz (THz) technology has many potential applications in numerous fields such as spectroscopy, imaging, quality assurance and homeland security [93–95]. One of the most attractive tools for terahertz application is the Laser Terahertz Emission Microscopy (LTEM) [101,102]. With the rapid development of LTEM technology, the ability to investigate super-current distribution, ferroelectric domains and microprocessors, the development of a scanning probe type LTEM and the one of THz cameras utilizing photoconductor arrays, bolometers and superconducting tunnel junctions make the LTEM expandingly used in the field of photovoltaic cells [98,99].

LTEM images allow the visualization of the crystalline grain structure of the solar cell and the dynamics of photocarriers. They render the local electric field distribution in the cell. LTEM emerges therefore as a promising technique for the evaluation and the inspection of solar cells [103].

Nakanishi et al. [104] employed a laser terahertz emission microscope (LTEM) as a novel tool for evaluating solar cells. Through their research, THz emission can be observed without electrical contacts.

These results shed light on the feasibility of LTEM for application as a noncontact inspection technique that evaluates the conversion efficiency and the dynamics of excited carriers in photovoltaic cells.

Salek et al. investigated the effects of continuous wave laser illumination on terahertz emissions from a polysilicon solar cell. The results highlighted that terahertz waves were attenuated in the presence of illumination by a cw laser. These modifications are related to the numbers of free carriers in the solar cell and can be explained in terms of screening of the electric field in the depletion layer of the PN junction, as a result of the presence of photoexcited carriers. They also throw into evidence that the amplitude of the terahertz emission depends on the wavelength of the illumination laser and is smaller for a short wavelength laser as a result of surface recombination. The findings of these experiments suggest that LTEM could be a useful technique for analyzing and inspecting solar cells [101].

6.1.7. Machine vision

Machine vision relies on the machine instead of on the human eyes to measure and judge [100,105]. The machine vision system by means of machine vision products (image capture devices, include CMOS and CCD) will be converted into the target image signal and sent to a dedicated image processing system according to the pixel distribution and to the brightness, and the colour information into digital signals.

This technology is amply used in the discovering of flaws in polysilicon solar wafers [106,107]. The detection of invisible microcracks in multicrystalline silicon solar wafers is very problematic because of the heterogeneously textured backgrounds of the wafers. The challenge is twofold. First, invisible microcracks must be visualized to image devices. Secondly, an image processing sequence capable of extracting microcracks from the captured images must be developed [105].

6.1.8. Impact testing

The acoustic measurements are obtained by mechanically exciting vibratory modes in single-crystalline silicon wafers to notice the location and the types of microcracks [108]. This method depends on the

audible impact response from cracked wafer sounds which differs from an uncracked wafer.

The setup is based on applying impacts to the wafer utilizing a miniature piezoelectric impact hammer with a vinyl tip, bearing a weight of 2.9 g and a length of 10 cm, generating waves with up to 2 000 Hz frequency [108]. The impact response is measured with a microphone mounted at 2 cm above the test wafer. The reported results display the dependence of the natural frequencies, the peak amplitudes and the damping levels with the crack type and its location. However, the force applied during impact tests can cause cracks, even in intact cells. This approach is uniquely used to detect facial fissures with a total length of only 10 mm.

6.2. Materials investigation and cross-sectioning techniques

The cell or the wafer is broken down in order to determine the mechanical properties such as strength, toughness and hardness to find out for example if the quality of a weld is good enough to withstand extreme pressure or to verify the properties of a material.

6.2.1. Scanning Electron Microscopy (SEM)

This method (SEM) is the most accessed one among other electronic microscopes because of its high resolution and its particular advantage of providing great depth field which enables obtaining images of the sample surface with a 3D appearance and if possible the chemical composition.

The electron beam is created by an electron gun and is passed through lenses of electromagnetic nature and apertures that diminish the diameter of the beam focusing on the surface of the sample and diverging in its path.

The beam is deflected by two pairs of electromagnetic coils allowing the probe to move along a line in the surface and to change the location to a next one so as to scan a new line [109].

6.2.2. Focused Ion Beam (FIB) microscopy

This technique (FIB) is suitable for metals, polymers, ceramics, composites, fibre/powder and semiconductors. Biological, geological applications and pharmaceuticals can also be handled with it [110].

FIB uses an ion beam to interact with the specimen. The interaction is similar for the electrons with the SEM technique but owing to the difference in the size, the interaction between ions and atoms is higher than that between atoms and electrons producing a decrement in the energy of ions and in the penetration depth.

7. Summary and discussion

The above-mentioned studies on cracks in photovoltaic cells and the methods to characterize them are synthesized in Tables 1 and 2 respectively.

7.1. Characteristics, tests and impact of cracks

The main studies presented about cracked cells in photovoltaic modules are included in Table 1. For each study, the essential results, the observations or conclusions are indicated with the techniques used to induce fissures or to detect them.

7.2. Detection methods

Non-destructive methods are compared in Table 2 namely the most used and the most promising ones either in the photovoltaic cell industry or in the supervision and in the control of photovoltaic installations.

For the cross sectioning technique, the use of FIB offers several advantages over other techniques. While cleaving or dicing and polishing for SEM investigations take several hours, FIB permits cross sections to be realized within just a few minutes. Also, with FIB it is possible to figure out the precise location of the cross section. An arbitrary number of subsequent cross section ‘slices’ can be accounted for on the same sample [114].

7.3. Proposed solutions

To mitigate the effects of cracks in the photovoltaic panels, the formation of cracks has to be warded off and the prevention of thermal fatigue, cyclic and mechanical load requires to be anticipated. Also the design of a metallic grid or of a new structure unaffected by the cell cracks could reduce their effect.

Researchers are trying to find and propose solutions to avoid or reduce the appearance of cracks and their propagation tendency. Their results highlight a relationship between the thickness of the solar cell and the criticality of cracks [115]. The effect is more important on thinner cells although the photovoltaic industry tends to reduce them. Hence, one of the solutions would consist in developing a technology that meets the mechanical requirements necessary to satisfy this reduction.

Another solution would be to limit the defects and to improve the quality of the materials used in solar cells by minimizing the material-induced defects such as defects in the structure of a grain boundary or by avoiding recombination due to a crystalline defects induced by the manufacturing process through aluminium particles or scratches [116,117].

Concerning the design, Kajari-Schröder et al. discussed a new strategy for reducing the risk of loss in the power output of the photovoltaic modules. A 90° rotation of the busbars would not affect the frequency of cracks and has the potential to lessen the criticality of the generated cracks by up to 50% [20]. Increased number of bypass diodes in the photovoltaic modules enable to protect them against damaged and shaded cells [118] or adding more busbars, to bring them up to 4 or 5, could also be a relevant solution. Nevertheless, this raise in the number of busbars has the downside potential of creating a larger number of open cracks per module [119].

Another strategy is proposed to use a more flexible cell metallization preventing electrical isolation of the cell parts in the case of a broken silicon in order to reduce the influence of cracking and to favour the thermal stability of the constituent materials used in the photovoltaic module [40]. The optimal design of the structure of the photovoltaic module requires the accounting of thermal expansion [42].

Results show that the cyclic strain deformation typically induced by temperature variation in European climate zones implies a significant amount of plasticity in the busbars and a substantial residual strain [120]. The broadening of the cell spacing to curtail the value of the applied cyclic strain could be a practical solution to abate the occurrence of the plastic deformation and to keep back the failure of the busbars [116].

Table 1. Contributions of the studies on cracked photovoltaic modules

	Techniques used	Essential results, conclusions or observations	Ref.
2006	Electroluminescence Thermal cycle	Electrical impact on cell cracks originates from an interruption of the front-side contact network. Continued thermal cycling weakens the grid finger intersected by the crack line. Determination of the probability of a grid finger discontinuation. Calculation of the associated loss for the cell area.	[111]
2010	Thermography Electroluminescence image Thermal cycling Mechanical analysis	Existence of cracks at the busbars and cracks starting at other points of the cell. Soldering induces high stress in the silicon cell concentrated at the end of the solder area. Lamination process critical for crack initiation. Predominant microcrack in the busbar and in the soldered interconnectors.	[35]
2011	Mechanical load test (IEC 61215 10.16) Statistical and numerical analysis Electroluminescence image	Strong dependence between the criticality of cracks and their orientations. Statistical distribution of crack orientations. Cracks parallel to the busbars appear more frequently.	[20]
	Electroluminescence Mechanical load test Humidity freeze test Simulation model	Risk of power loss under 2.5% caused by microcracks after mechanical load testing. Increase of the resistance between cracked cell fractions subsequent to accelerated test. Correlation between the number of cracked cells and the power degradation ensuing accelerated aging test.	[40]
2012	Mechanical load test Artificial aging (200 humidity-freeze cycles) Electroluminescence image	High criticality on the output power of cracks parallel to the busbars. High propagation probability under artificial aging for cracks parallel to the busbars and for cracks in several directions.	[32]
	Electric model Electroluminescence	Obtention of I-V curves by classifying the patterns into three shapes according to the direction of the cracks and by simulating them. Error close to 3% for the simulation results regarding the actual measured output values. Continuous development of the microcrack of a solar cell under thermal stress due to the change of temperature.	[42]
2013	Electroluminescence SEM microscopy Mechanical load test Artificial aging (200 thermal cycling test)	Appearance of two distinct types of dark areas after IEC test: - irregularly shaped regions as a result of cracks in the silicon wafers - regular rectangular shaped cracks on account of disconnected fingers at the finger–busbar intersection (in poorly welded regions of the silicon wafer)	[33]
	Electric model Computational method	Determination of the electrically inactive area from the analysis of the microcrack pattern. Capability of the method to analyze the orientation and the distribution of microcracks, and equally the effect of cracking on the electrical characteristics. Numerical implementation revealing that the proposed approach can be applied to the real case.	[44]
2014	Strength testing (4-point-bending test) Electroluminescence	Strength and breakage of solar cells depending strongly on the side and on the direction of loading caused by the metallization structure. Lowest strength detected for the backside being loaded with tensile stress	[34]

	Techniques used	Essential results, conclusions or observations	Ref.
	SEM microscopy	parallel to the busbars.	
	SEM microscopy Thermal cycle Finite element (FE) analysis	Impact of the thermal fatigue along the grain boundary of the welding on the interconnection between the soldering copper and the silver metallization. Growth of the series resistance under each processing condition concerning a thermal cycle. Changes of the average normalized maximal power as a function of the thermal cycle.	[26]
2015	Crack statistics Monte Carlo simulations	Estimation of the power loss of the photovoltaic modules between 6 and 22% with field data. Calculation of the parameters of the distribution of output powers for equivalent break resistance values. Break resistance values not known with certainty in the real cases.	[43]
2016	Electroluminescence Electric model Vickers tests	Novel electric model with spatially varying distributed resistance (DR) accounting for damage in the material surrounding a channel crack to predict the current through the thickness of cracked silicon solar cells, as well as the current and the voltage along the grid line.	[112]
	Electroluminescence Photoluminescence SEM microscopy Electron-beam induced current	Cracks above 4 mm^2 leading to severe shunts with high probability. Shunts with very low parallel resistance in Cz-Si solar cells attributed to metal-to-metal contacts between front and rear sides of the solar cell. Reduced robustness of Cz-Si compared with mc-Si with regard to the formation of shunts at microcracks stemming from a widening of the crack channels above 10 μm in alkaline texturing, facilitating the formation of metal-to-metal contacts.	[113]
2017	Electroluminescence Statistical analysis Surface analysis	No cracks for 15.6% of the overall photovoltaic modules examined. Important impact on the total amount of power generated by photovoltaic modules by 60% out of 84.4% of the arrays.	[45]

Table 2. Comparison for NDT methods

	NDT techniques	Advantages	Disadvantages	Ref.
Electrical	DC/AC electrical parameters	High detection speed Detection of DC and AC electrical parameters Comprehension of the measuring parameters	Restricted to theoretical analysis	[42,49, 51,52, 54]
	Laser beam induced current (LBIC)	Powerful device for mapping distribution of recombination active defects and impurities in solar cells	Slow detection speed Need for electrical contacts Scanning to be performed for the entire wafer area	[56,61]
	Electron beam induced current (EBIC)	Convenient device for finding sub-surface and other difficult-to-see damage areas	Slow detection speed Limited scope of application	[62,63]
	High critical temperature superconductor superconducting quantum interference device (HTS-SQUID)	High sensitivity High bandwidth High resolution	Expensive equipment Inconvenient operation	[64–66]
Ultrasonic and	Scanning acoustic microscopy (SAM)	High detection accuracy High sensitivity (5-10 μm cracks)	Long acquisition time (10-15 min) Used as a standalone tool Necessitates a special sample preparation (covering the wafer with water)	[18,71]
	Resonance ultrasonic vibration (RUV)	High throughput High detection speed Non-contact method	Low sensitivity to crack length and location	[121, 122]

	NDT techniques	Advantages	Disadvantages	Ref.
	Lamb wave air coupled ultrasonic testing (LAC-UT)	High throughput Large detection area	Needs the usage of a coupling agent Difficult to achieve fast in-service detection	[74–76]
Optic	Electronic speckle pattern interferometry (ESPI)	No interference between cracks and scratches	Low detection depth Low detection accuracy	[77–80]
Thermal	Illuminated lock-in thermography (LIT)	High resolution imaging of defect Non-contact method	Long acquisition time Offline inspection only Suffers from thermal blurring	[82–88]
Thermal	Ultrasound lock-in thermography (ULIT)	High resolution imaging of crack Non-contact method Used with wafers and solar cells	Long acquisition time (30 min) Expensive advanced thermal imager Requires a special sample preparation (covering surface of wafer with black paint)	[123–125]
Short-Wave Infrared (SWIR)	Electroluminescence (EL)	High throughput No special sample preparation	Necessitates external power supply Imaging resolution limited by wavelength Used only with finished solar cells Interferences with other defects such as scratches	[93–96]
Short-Wave Infrared (SWIR)	Photoluminescence (PL)	High throughput Non-contact method Used with wafers and solar cells	Necessitates light source excitation Imaging resolution limited by wavelength Used only with finished solar cells Interferences with other defects such as scratches	[97,98]
Short-Wave Infrared (SWIR)	Quantitative lock-in carrierography (LIC)	High spatial resolution Non-contact method	Long acquisition time	[85,100]
TeraHz	Laser terahertz emission microscope (LTEM)	Very advanced spatial resolution compared to conventional terahertz imaging	Highly-priced equipment Immature technology	[101,102,104–107]
Mechanical	Impact testing	High throughput	Impacts could introduce cracks Detects cracks with total length of only 10 nm	[126–129]

8. Conclusion

The most significant information available on cracks in solar cells and photovoltaic modules, their impact on the efficiency and the detection techniques used have been reviewed. The main conclusions are as follows:

- The cracks either within the silicon wafers or in the ribbon bar intersection do not necessarily affect the power of a photovoltaic module. However, research studies point out that cracked photovoltaic modules suffer from a lower stability of energy production under the effect of artificial aging and the same runs for photovoltaic modules installed in fields. Cracks induced by the production process of the photovoltaic modules should be avoided as much as possible, by reason that they serve as starting points for the propagation of the cracks during operating even under very small amplitudes of stress.
- Current qualification tests are not sufficient to estimate the damage caused by cracking and the module lifetime under field conditions making this task more difficult to envisage the worldwide operating of photovoltaic systems in all climate zones with different configurations.
- The different technologies of detection: acoustic, ultrasonic, optical, electromagnetic, thermal, eddy and infrared testing of silicon solar cells have been reviewed. The future of solar cells and material efficiency depends on the evolution of these detection technologies that are helpful for the advancement towards rapid detection, quantitative detection and fine evaluation especially with non-destructive methods. These technologies must take into account the variety of parameters to be measured and the complex structure of the detection site.
- Scientific researchers and the photovoltaic industries, among the existent technologies, use more the luminescence technology (EL and PL) not suffering from thermal blurring, less expensive and usually requiring a lower acquisition time than the others. A luminescence device provides high quality results but choosing between

EL and PL techniques, PL is better than EL as it can be applied for solar wafers and equally for solar cells.

- Non-destructive tests highlight if cracks, corrosion or other faults exist while destructive tests in turn indicate how and when the objects are in danger of breakdowns or failures.
- A promising technique that combines non-destructive and destructive methods that would meet the needs of various types of solar cell defects, rapid and quantitative detection, non-contact and fine determination could be developed in future works.

The development of a model associated with the various parameters in terms of cracking will be an attractive domain of research to perfect the knowledge of the behaviour of photovoltaic modules during their life cycle under the consequences of degradation modes.

Acknowledgments

The authors wish to extend their great gratitude to Mrs. Wilhelmina Logerais, a native English speaker, for her particular help during the entire process of paper composing and revising.

References

[1] International Renewable Energy Agency (IRENA), A Roadmap for 2050, (2018).
[2] M. A. Green, K. Emery, Y. Hishikawa, W. Warta, E. D. Dunlop, Prog. Photovoltaics Res. Appl. **24**, 905 (2016).
[3] S. Zhang, X. Pan, H. Jiao, W. Deng, J. Xu, Y. Chen, P. P. Altermatt, Z. Feng, P. J. Verlinden, IEEE J. Photovoltaics **6**(1), 145 (2016).
[4] B. Parida, S. Iniyan, R. Goic, Renew. Sustain. Energy Rev. **15**, 1625 (2011).
[5] A. Morales-Acevedo, Sol. Energy **80**, 675 (2006).
[6] N. Ali, A. Hussain, R. Ahmed, M. K. Wang, C. Zhao, B. U. Haq, Y. Q. Fu, **59**, 726 (2016).
[7] R. W. Weaver, R. H. Lee, J. D. Meyer, L. D. Runkle, FSA Field Test Annual Report, California, 1984.
[8] E. Cuddihy, C. Coulbert, A. Gupta, R. Liang, Flat-plate Solar Array Project Final Report Volume VII : Module Encapsulation, California, 1986.
[9] L. André, P. Henri, Evaluation et maîtrise du vieillissement industriel, Ed. by Tec & Doc Lavoisier, 2005.
[10] M. Köntges, S. Kurtz, C. Packard, U. Jahn, K. A. Berger, K. Kato, T. Friesen, H. Liu, M. Van Iseghem, Review on Failures of Photovoltaic Modules, Report IEA-PVPS T13-01:2013, 2013.
[11] O. O. Ogbomo, E. H. Amalu, N. N. Ekere, P. O. Olagbegi, Renew. Sustain. Energy Rev. **75**, 1225 (2017).
[12] A. Gabor, M. Ralli, S. Montminy, L. Alegria, C. Bordonaro, J. Woods, L. Felton, 21st Eur. Photovolt. Sol. Energy Conf., 2006.
[13] P. S. Dominguez, J. M. Fernandez, in: Proc. 20th Eur. Photovolt. Sol. Energy Conf., Barcelona, Spain, 2005.
[14] P. A. Wang, Conf. Rec. 2006 IEEE 4th World Conf. Photovolt. Energy Conversion, WCPEC-4 **1**, 1179 (2007).
[15] M. Sander, S. Dietrich, M. Pander, S. Schweizer, M. Ebert, J. Bagdahn **8112**, 811209 (2011).
[16] W. J. R. Song, S. K. Tippabhotla, A. A. O. Tay, A. S. Budiman. Sol. Energy Mater Sol. Cells **187,** 241 (2018).
[17] F. Reil, K. Strohkendl, J. Althaus, W. Vaassen, Mechanische Beanspruchungen fur PV-Module Transportbelastungen, Köln, 2009.
[18] W. Dallas, O. Polupan, S. Ostapenko, Meas. Sci. Technol. **18**, 852 (2007).
[19] J. H. Wohlgemuth, D. W. Long. In Conf. Rec. 2006 IEEE 4th World Conf. Photovolt. Energy Conversion, WCPEC-4, 2006.
[20] S. Kajari-Schröder, I. Kunze, U. Eitner, M. Köntges, Sol. Energy Mater. Sol. Cells **95**, 3054 (2011).
[21] B. Weinreich, B. Schauer, M. Zehner, G. Becker, Validier ung der Ver messung gebr ochener Zellen im Feld mittels Leistungs-PV-Ther mogra fie, in: Proc. 27th Symp. Photovolt. Sol. Energy, Bad Staffelstein, 190 (2012).
[22] J. A. Gow, C. D. Manning, IEE Proc. - Electr. Power Appl. **146**, 193 (1999).
[23] D. Sera, R. Teodorescu, P. Rodriguez, IEEE Int. Symp. Ind. Electron., 2392 (2007).
[24] K. Benlarbi, L. Mokrani, M. S. Nait-Said, Sol. Energy **77**, 203 (2004).
[25] P. Rajput, G. N. Tiwari, O. S. Sastry, B. Bora, V. Sharma, Sol. Energy **135**, 786 (2016).
[26] N. Park, J. Jeong, C. Han, Microelectron. Reliab. **54**, 1562 (2014).
[27] Y.-C. Chiou, J.-Z. Liu, Y.-T. Liang., Sens. Rev. **31**, 154 (2011).
[28] V. Sharma, S. S. Chandel, Renew. Sustain. Energy Rev. **27**, 753 (2013).
[29] IEC 61215, Crystalline silicon terrestrial photovoltaic (PV) modules - Design qualification and type approval, 2005.
[30] J. Wendt, M. Träger, M. Mette, A. Pfennig, B. Jäckel, 24th EU Photovolt. Spec. Conf., 3420 (2009).
[31] M. Paggi, I. Berardone, A. Infuso, M. Corrado, Journal of Energy Challenges and Mechanics **1**(1), 20 (2014).
[32] S. Kajari-Schröder, I. Kunze, M. Köntges, Energy Procedia **27**, 658 (2012).
[33] P. Chaturvedi, B. Hoex, T. M. Walsh, Sol. Energy Mater. Sol. Cells **108**, 78 (2013).
[34] F. Kaule, W. Wang, S. Schoenfelder, Sol. Energy Mater. Sol. Cells **120**, 441 (2014).
[35] M. Sander, B. Henke, H. Schwarz, S. Dietrich, S. Schweizer, M. Ebert, Syst. III **7773**, 777308 (2010).
[36] M. Paggi, A. Sapora, Energy Procedia **38**, 506 (2013).
[37] J. Tracy, N. Bosco, R. Dauskardt, IEEE J. Photovoltaics **7**(6), 1635 (2017).
[38] D. C. Jordan, C. Deline, S. R. Kurtz, G. M. Kimball, M. Anderson, IEEE J. Photovoltaics **8**, 525 (2018).

[39] A. Ndiaye, A. Charki, A. Kobi, C. M. F. Kébé, P. A. Ndiaye, V. Sambou, Sol. Energy **96**, 140 (2013).
[40] M. Köntges, I. Kunze, S. Kajari-Schröder, X. Breitenmoser, B. Bjørneklett, Sol. Energy Mater. Sol. Cells **95**, 1131 (2011).
[41] R. Subrahmanyan, J. R. Wilcox, C. Y. Li, IEEE Trans. Components, Hybrids, Manuf. Technol. **12**, 480 (1989).
[42] Y.-H. Song, G.-H. Kang, G.-J. Yu, H.-G. Ahn, D.-Y. Han, Trans. Korean Inst. Electr. Eng. **61**, 407 (2012).
[43] A. Morlier, F. Haase, K. Marc, IEEE J. Photovoltaics **5**, 1735 (2015).
[44] M. Paggi, M. Corrado, M. A. Rodriguez, Compos. Struct. **95**, 630 (2013).
[45] M. Dhimish, V. Holmes, B. Mehrdadi, M. Dales, J. Sci. Adv. Mater. Devices **2**, 199 (2017).
[46] H. C. Liu, C.-T. Huang, W.-K. Lee, S.-S. Yan, F.-M. Lin, Energy Power Eng. **07**, 348 (2015).
[47] A. Dolara, G. C. Lazaroiu, S. Leva, G. Manzolin, L. Votta, IEEE J. Photovoltaics **6**, 1269 (2016).
[48] D. J. Crain, S. E. Rock, J. E. Garland, D. Roy, Curr. Appl. Phys. **13**, 2087 (2013).
[49] J. C. Wang, J. C. Shieh, Y. L. Su, K. C. Kuo, Y. W. Chang, Y. T. Liang, J. J. Chou, K. C. Liao, J. A. Jiang, Energy **36**, 5968 (2011).
[50] D. Chenvidhya, K. Kirtikara, C. Jivacate, Sol. Energy Mater. Sol. Cells **80**, 459 (2003).
[51] D. Chenvidhya, C. Limsakul, J. Thongpron, K. Kirtikara, C. Jivacate, Proc. 14th Int. Photovolt. Sci. Eng. Conf, 1 (2004).
[52] J. Thongpron, K. Kirtikara, C. Jivacate, Sol. Energy Mater. Sol. Cells **90**, 3078 (2006).
[53] K. A. Kim, G. S. Seo, B. H. Cho, P. T. Krein, IEEE Trans. Power Electron. **31**, 1121 (2016).
[54] D. Chenvidhya, K. Kirtikara, C. Jivacate, Sol. Energy Mater. Sol. Cells **86**, 243 (2005).
[55] D. T. Cotfas, P. A. Cotfas, S. Kaplanis, Renew. Sustain. Energy Rev. **61**, 213 (2016).
[56] J. Carstensen, G. Popkirov, J. Bahr, H. Föll, Sol. Energy Mater. Sol. Cells **76**, 599 (2003).
[57] B. Moralejo, M.A. González, J. Jiménez, V. Parra, O. Martínez, J. Gutiérrez, O. Charro, J. Electron. Mater. **39**, 663 (2010).
[58] F. J. Vorster, E. E. Van Dyk, Rev. Sci. Instrum. **78**, (2007).
[59] F. J. Vorster, E. E. van Dyk, Sol. Energy Mater. Sol. Cells **91**, 871 (2007).
[60] D. A. Redfern, C. A. Musca, J. M. Dell, L. Faraone, IEEE Trans. Electron Devices **52**, 2163 (2005).
[61] M. Israil, A. Ghani, Y. Kerm, Phys. Sci. Int. J. **4**, 1073 (2014).
[62] Y. Jin, S.T. Dunham, IEEE J. Photovoltaics **7**, 329 (2017).
[63] V. I. Orlov, E. B. Yakimov, Superlattices Microstruct. **99**, 202 (2016).
[64] M. C. De Andrade, A. L. De Escobar, B. J. Taylor, S. Berggren, B. Higa, S. Dinh, R. L. Fagaly, J. Talvacchio, B. Nechay, J. Przybysz, IEEE Trans. Appl. Supercond. **25**, 1 (2015).
[65] S. Topolovec, H. Krenn, R. Würschum, Rev. Sci. Instrum. **86**, (2015).
[66] Y. Nakatani, T. Hayashi, H. Itozaki, IEEE Trans. Appl. Supercond. **21**, 416 (2011).
[67] M. Darmon, V. Dorval, A. Kamta Djakou, L. Fradkin, S. Chatillon, Ultrasonics **64**, 115 (2016).
[68] E. Of, Y. For, EWSHM - 7th Eur. Work. Struct. Heal. Monit., 24 (2014).
[69] P. N. Bilgunde, L. J. Bond, 41st Annu. Rev. Prog. Quant. Nondestruct. Eval. (AIP Conf. Proc. 1650) **1650**, 1543 (2015).
[70] L. Golaski, NDT Assess. New Syst. Prestress. Concr. Struct., 7 (2004).
[71] A. Belyaev, O. Polupan, W. Dallas, S. Ostapenko, D. Hess, J. Wohlgemuth, Appl. Phys. Lett. **88**, (2006).
[72] Y. Emirov, A. Belyaev, D. Cruson, I. Tarasov, A. Kumar, H. Wu, S. Melkote, S. Ostapenko, Conf. Rec. IEEE Photovolt. Spec. Conf., 002161 (2011).
[73] L. Meng, S. S. P. Rao, C. S. Bhatia, S. E. Steen, A. G. Street, J. C. H. Phang, 2012 IEEE 38th Photovolt. Spec. Conf. PART 2, **3**, 1 (2013).
[74] S. K. Chakrapani, M. J. Padiyar, K. Balasubramaniam, J. Nondestruct. Eval. **31**, 46 (2012).
[75] O. Anspach, B. Hurka, K. Sunder, Sol. Energy Mater. Sol. Cells **131**, 58 (2014).
[76] K. Watanabe, M., Nishihira, M., Imano, Jpn. J. Appl. Phys. **45**, 4565 (2006).
[77] T. Statsenko, V. Chatziioannou, T. Moore, W. Kausel, Appl. Opt. **55**, 1913 (2016).
[78] E. A. Zarate, E. Custodio G., C. G. Treviño-Palacios, R. Rodríguez-Vera, H. J. Puga-Soberanes, Sol. Energy Mater. Sol. Cells **88**, 217 (2005).
[79] C.-C. Yin, T.-K. Wen, **8321**, 832139 (2011).
[80] M. Abdelhamid, R. Singh, M. Omar, IEEE J. Photovoltaics **4**, 514 (2014).
[81] P. N. Vinod, S. Joseph, R. John, Nondestruct. Test. Eval. **32**, 185 (2017).
[82] O. Breitenstein, Int. J. Nanoparticles **6**, 81 (2013).
[83] T. Y. Chung, C. H. Wang, K. J. Chang, S. Y. Chen, H. H. Hsieh, C. P. Huang, C. H. Arthur Cheng, J. Appl. Phys. **115**, (2014).
[84] O. Breitenstein, C. Shen, H. Kampwerth, M. A. Green, Energy Procedia **38**, 2 (2013).
[85] O. Breitenstein, Quant. Infrared Thermogr. J. **7**, 147 (2010).
[86] M. Kasemann, M. C. Schubert, M. The, M. Köber, M. Hermle, W. Warta, Appl. Phys. Lett. **89**, (2006).
[87] J. Adams, A. Vetter, F. Hoga, F. Fecher, J. P. Theisen, C. J. Brabec, C. Buerhop-Lutz, Sol. Energy Mater. Sol. Cells **123**, 159 (2014).
[88] J. Isenberg, A. S. H. Heide van der, W. Warta, 20th Eur. Photovolt. Sol. Energy Conf. 6-10 June 2005, Barcelona, Spain, 6 (2005).
[89] V. P. Vavilov, Proc. of SPIE, **9861**, 98610I (2016).
[90] Y. Wang, H. Ke, J. Shi, B. Gao, G. Tian, Proc. 2016 IEEE Far East NDT New Technol. Appl. Forum, FENDT 2016, 0 (2017).

[91] U. Netzelmann, G. Walle, S. Lugin, A. Ehlen, S. Bessert, B. Valeske, Quant. Infrared Thermogr. J. **13**, 170 (2016).
[92] U. Netzelmann, G. Walle, 17th WCorld Conf. NDT, Shanghai, China, 8 (2008).
[93] T. Fuyuki, A. Kitiyanan, Appl. Phys. A Mater. Sci. Process. **96**, 189 (2009).
[94] D. M. Tsai, S. C. Wu, W. C. Li, Sol. Energy Mater. Sol. Cells **99**, 250 (2012).
[95] W.-J. Lin, Y.-H. Lei, C.-H. Huang, Conf. Rec. - IEEE Instrum. Meas. Technol. Conf., 182 (2011).
[96] T. Fuyuki, H. Kondo, T. Yamazaki, Y. Takahashi, Y. Uraoka, Appl. Phys. Lett. **86**, 1 (2005).
[97] T. Trupke, R. A. Bardos, M. D. Abbott, F. W. Chen, J. E. Cotter, A. Lorenz, Conf. Rec. 2006 IEEE 4th World Conf. Photovolt. Energy Conversion, WCPEC-4 **1**, 928 (2007).
[98] M. Israil, S. A. Anwar, M. Z. Abdullah, Trans. Inst. Meas. Control **35**, 606 (2013).
[99] J. Haunschild, I. E. Reis, T. Chipei, M. Demant, B. Thaidigsmann, M. Linse, S. Rein, Sol. Energy Mater. Sol. Cells **106**, 71 (2012).
[100] A. Mandelis, Y. Zhang, A. Melnikov, J. Appl. Phys. **112**, 1 (2012).
[101] K. A. Salek, Opt. Eng. **53**, 031204 (2013).
[102] B. H. Murakami, N. Uchida, R. Inoue, S. Kim, T. Kiwa, M. Tonouchi, 374007 (2015).
[103] M. Tonouchi, Nat. Photonics **1**, 97 (2007).
[104] N. Hidetoshi, F. Shogo, T. Kazuhisa, K. Iwao, M. Hironaru, T. Masayoshi, Appl. Phys. Express **5**, 112301 (2012).
[105] S. Yang, P. Du, Y. Sun, **10030**, 1003029 (2016).
[106] D. Saeedkia, Handbook of terahertz technology for imaging, sensing and communications, Elsevier, (2013).
[107] R. M. Woodward, Proc. SPIE **5781**, 22 (2005).
[108] C. Hilmersson, D. P. Hess, W. Dallas, S. Ostapenko, Appl. Acoust. **69**, 755 (2008).
[109] Yang Leng, Materials Characterization: Introduction to Microscopic and Spectroscopic Methods, 2008.
[110] F. A. Giannuzzi, Lucille A. Stevie, Introduction to Focused Ion Beams: Instrumentation, Theory, Techniques and Practice, SPRINGER, 2005.
[111] C. G. Zimmermann, IEEE Trans. Device Mater. Reliab. **6**, 486 (2006).
[112] M. Paggi, I. Berardone, M. Martire, Energy Procedia **92**, 576 (2016).
[113] M. Demant, T. Welschehold, S. Kluska, S. Rein, IEEE J. Photovoltaics **6**, 136 (2016).
[114] S. Reyntjens, R. Puers, J. Micromechanics Microengineering **11**, 287 (2001).
[115] G. Coletti, N. J. C. M. van der Borg, S. De Iuliis, C. J. J. Tool, L. J. Geerligs, 21st Eur. Photovolt. Sol. Energy Conf. Exhib., (2006).
[116] G. Acciani, O. Falcone, S. Vergura. In Proc. Int. Symp. Ind. Electron. Conf., 2745 (2010).
[117] A. Schieferdecker, J. Sachse, T. Mueller, U. Seidel, L. Bartholomaeus, S. Germershausen, R. Perras, R. Meissner, H. Hoebbel, A. Schenke, K. Bhatti, K. H. Küsters, H. Richter, Phys. Status Solidi C **8**(3), 871 (2011).
[118] A. J. Carr, M. J. Jansen, M. De Bruijne, L. Okel, M. Kloos, W. Eerenstein, 2685 (2014).
[119] A. M. Gabor, R. Janoch, A. Anselmo, H. Field, NREL PV Modul. Reliab. Work. Denver, CO USA, 1 (2015).
[120] C. Borri, M. Gagliardi, M. Paggi, Sol. Energy Mater. Sol. Cells, (2018).
[121] L. Meng, D. Nagalingam, C. S. Bhatia, A. G. Street, J. C. H. Phang, Sol. Energy Mater. Sol. Cells **95**, 2632 (2011).
[122] Z. Y. Xu, S. Y. Gao, J. Huang, Y. Wang, Adv. Mater. Res. **764**, 9 (2013).
[123] A. Dillenz, G. Busse, D. Wu, Proc. SPIE 3827, Diagnostic Imaging Technologies and Industrial Applications, (1999).
[124] J. P. Rakotoniaina, O. Breitenstein, M. H. Al Rifai, D. Franke, A. Schneider, in Proc. PV Sol. Conf., Paris, France, 640 (2004).
[125] T. Qingjua, L. Junyan, W. Yang, L. Huia, Procedia Engineering **16**, 499 (2011).
[126] I. Publishing, Z. Yinong, P. Jiantao, F. Jianjun, **179**, 157 (2014).
[127] M. L. Feng, X. J. Zhou, J. G. Yu, Adv. Mater. Res. **718–720**, 532 (2013).
[128] Y. Chiou, J. Liu, Y. Liang, Sens. Rev. **31**, 154 (2011).
[129] D. M. Tsai, M. C. Lin, Robot. Comput. Integr. Manuf. **29**, 312 (2013).

*Corresponding authors: ennemriamina@gmail.com
logeraispo@gmail.com